The 9th European Congress on Computational Methods in Applied Sciences and Engineering
ECCOMAS Congress 2024
3–7 June 2024, Lisboa, Portugal

EXTRA CORPOREAL MEMBRANE OXYGENATION SUPPORT FOR PERFUSION IN CARDIAC SHOCK: A COMPUTATIONAL ANALYSIS

E. VIGNALI[1], E. GASPAROTTI[1], M. MAZZOLI[1,2], D. HAXHIADEMI[3] AND S. CELI[1]

[1] BioCardioLab, Bioengineering Unit
Fondazione Toscana Gabriele Monasterio, Massa, Italy
e-mail: evignali@ftgm.it, gasparotti@ftgm.it, mmazzoli@ftgm.it, s.celi@ftgm.it

[2] Department of Information Engineering
University of Pisa, Pisa, Italy

[3] Anesthesia and Intensive Care Unit
Fondazione Toscana Gabriele Monasterio, Massa, Italy
e-mail: dorela@ftgm.it

Key words: Veno-Arterial Extracorporeal Membrane Oxygenation, Life Support Devices, cardiac Shock, Computational Fluid Dynamics, Aortic Hemodynamics, Vessel Perfusion, Afterload

Summary. The Veno-Arterial Extracorporeal Membrane Oxygenation (VA-ECMO) is a support procedure to provide oxygenated blood to patients affected by cardiogenic shock. Despite its widespread adoption, this support system hides some pitfalls and a deeper understanding of some phenomena is still required. In particular, it is well known that high levels of ECMO support grant vessel perfusion but also produce unwanted afterload increases. It would be suitable to have a tool to define an ECMO trade-off level to grant the sufficient perfusion and limit the afterload increase at minimum. The current study proposes a Computational Fluid Dynamic (CFD) approach to model a patient-specific VA-ECMO case. In particular, a total of three cases of cardiogenic shock (30%, 50% and 70% reduction of cardiac output), with ECMO support levels ranging from 0 to 9 l/min were setup. The results were evaluated in terms of mixing zone, afterload and flow perfusion at the different aortic vessels. The output data were, at last used to define a model for the estimation of an ECMO trade-off level, by considering the perfusion of each artery and the minimum possible increase of afterload.

1 INTRODUCTION

The condition of cardiogenic shock (CS) consists in a significant limitation of the healthy cardiac output (CO). This condition is usually a consequence of a myocardial infraction, in which the left ventricle (LV) has partially lost its functionality [1]. To manage the CS, different support devices are available in the clinical environment. The Veno-Arterial Extracorporeal Membrane Oxygenation (VA-ECMO) represents a valid clinical support system for the cardiopulmonary re establishment [2], providing a temporary mechanical circulatory support for patients affected by CS. The main principle behind the VA-ECMO is the usage a rotary pump to draw blood from

the venous circulation, force it through an oxygenator and then pump it back into the arterial circulation, in order to provide newly oxygenated blood to the body. The access to the arterial section is obtained by proceeding with the cannulation which can be at different levels of the circulation, including the lower body access via iliac artery. Despite its widespread adoption in the clinical context [3, 4], it is well established that VA-ECMO hides some drawbacks and pitfalls. The formation of a blood mixing zone between native (from LV) and support (from ECMO) blood flow has been observed in the clinical context [5]. The existence of this mixing zone, i.e. the watershed zone, is linked to the retrograde nature of ECMO flow and the consequent unbalancing of the blood perfusion in the different areas of the body. The presence of this zone is at the basis of differential hypoxemia usually occurring in patients during the VA-ECMO support (Harlequin syndrome) [6]. Most importantly, it is known that VA-ECMO with high support levels grants vessel perfusion but induces unwanted afterload increases [7]. This negative effect is another consequence of the retrograde nature of the flow from the ECMO system. To solve the issue of afterload increase linked with ECMO support, different LV unloading techniques are proposed in the clinical practice [8].
In the given context, it is clear that a deeper understanding of these phenomena linked with the VA-ECMO support plays a key role. Engineering approaches such as Computational Fluid Dynamic (CFD) simulations represent a valid tool to explore this environment, as also demonstrated for different cardiovascular districts [9, 10, 11]. In literature, it is possible to find numerous contributions for numerical modeling of VA-ECMO systems. It is worth reporting some groups focusing their attention on the behavior of the watershed zone [12, 13] and on the different strategies for cannulation [14, 15]. There are also some studies corroborating the numerical results with experimental evidences [16]. Nevertheless, sometimes it is worth underlining that some model limitations were not overcome, such as the adoption of idealized geometries for the aorta and simplified boundary conditions for the outlets [12, 17]. As an additional point, it appears that the state of the art lacks contributions concerning the afterload / perfusion balance issue. Only few manuscripts put the focus of their numerical models on this relevant clinical problem [18, 19]. A trade-off level of ECMO support, to simultaneously grant the overall perfusion and avoid unnecessary afterload increases, is still to be explored.
Starting from this context, the objective of the current manuscript is to propose a CFD model for the analysis of a patient specific case under different VA-ECMO support conditions. In particular, the aortic geometry was obtained by processing a patient-specific computed tomography (CT) dataset. A total number of 31 cases was simulated by varying the cardiogenic shock and the ECMO support levels, ranging from 30% to 70% CO reduction and from 0 l/min to 9 l/min, respectively. The healthy condition, assumed as the reference baseline, was simulated as well. The results were evaluated in terms of watershed zone position, afterload and perfusion of the different aortic vessels. At last, the results were successfully used to present a preliminary model for the estimation of an ECMO trade-off level. This level was defined by considering the perfusion of each aortic outlet on the basis of the healthy baseline and, thus, avoiding unwanted afterload increases.

2 MATERIALS AND METHODS

In this section, the main steps for the numerical workflow are summarized, including the simulation setup, the defined test cases and the output parameters, including the ECMO trade-off

level definition.

2.1 Numerical simulations setup

Firstly, the aortic geometry for the simulations was defined. A contrast-enhanced CT total body dataset of a patient-specific case was considered to this purpose. The dataset was processed by applying a semi-automatic segmentation algorithm to obtain the full aortic geometry. The aorta was considered by including the aortic root, the arch and the descending section. The following arteries were considered: brachiocephalic (BCA), left common carotid (LCCA), left common subclavian (LCSA) and left - right iliac (LIA - RIA) arteries (Figure 1a).

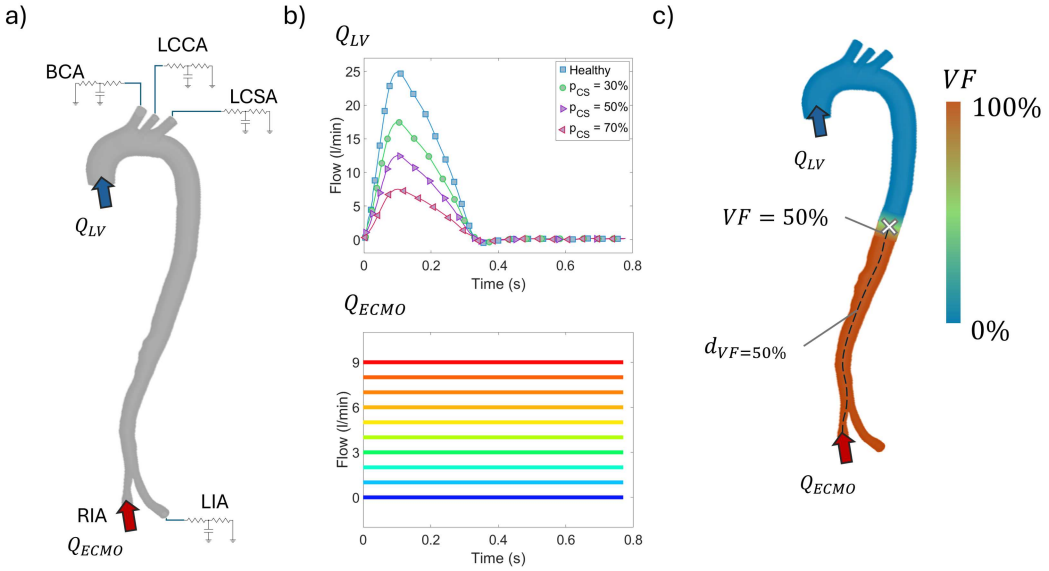

Figure 1: Setup for the CFD simulations (a), summary of inlet conditions (Q_{LV} and Q_{ECMO}) for the definition of the test cases (b) and example of watershed zone definition in terms of volume fraction (VF) and position ($d_{VF=50\%}$) (c).

After defining the aortic geometry, the CFD simulation was setup. The analysis was carried out with ANSYS Fluent software (Canonsburg, Pennsylvania, USA). The aortic domain was discretized with a mesh with water-tight polyhedral elements, including four inflation layers (growth-rate of 1.2 and a total thickness of 1.5 mm) for a total of 1.2e6 elements. Concerning the boundary conditions, these are schematized in Figure 1a. For the inlet boundaries, a time-varying flow waveform (Q_{LV}) was imposed at the aortic valvular plane to simulate the native action of the LV, while a constant flow (Q_{ECMO}) was imposed at RIA level to simulate the support action of the ECMO. For the outlet boundaries, each aortic vessel was modeled by adopting a 0D model. In particular, the 3-element Windkessel analogue circuit was implemented to maintain a physiological pressure range [20, 21]. The 3-element model is constituted by a proximal resistance (R_p), a distal resistance (R_d) and a compliance (C). The parameters for each aortic vessel were tuned according to reach a physiological pressure range in the healthy baseline configuration, with a minimum - maximum pressure of 80 - 120 mmHg, respectively. For the fluid model, a two-phases Mixture model was adopted. The two phases were chosen

in order to allow the discernment of the LV and ECMO blood. Each phase was modeled as an incompressible non-Newtonian fluid with constant density of 1060 kg/m^3. A Carreau model with the following rheologic parameters was imposed for the viscosity: time constant equal to 3.3 s, power law index equal to 0.37, zero and infinite shear viscosities equal to 0.056 kg/ms and 0.0035 kg/ms, respectively [22]. For each test case, a total of 10 cardiac cycles was simulated in order to reach the dynamic regime.

2.2 Test cases

The test cases were defined on the basis of the different combinations of inlet conditions, namely the CS shock levels and VA-ECMO support levels. For shock levels, three different values were imposed by considering a percentage reduction of the healthy CO (p_{CS}): 30%, 50% and 70%. The resulting Q_{LV} waveforms imposed as inlet are summarized in Figure 1b. For the ECMO support levels, ten levels of constant flow were considered, ranging from $Q_{ECMO} = 0$ l/min (no support) up to $Q_{ECMO} = 9$ l/min (maximum support) (Figure 1b). By considering all the different combinations of Q_{LV} and Q_{ECMO} inlet conditions, a total of 30 pathological scenarios were simulated. As an additional case, the healthy condition (no shock level and $Q_{ECMO} = 0$ l/min) was simulated, to serve as a baseline for the establishment of the vessel perfusion.

2.3 Output parameters and ECMO trade-off level

The results were evaluated in terms of *watershed zone*, *afterload*, *flow perfusion* at the different aortic vessels and *ECMO trade-off level*.
For the characterization of the watershed zone, the percentage of volume fraction (VF) of ECMO blood was considered:

$$VF = \frac{V_{ECMO}}{V_{ECMO} + V_{LV}} \times 100 \tag{1}$$

where V_{ECMO} and V_{LV} are the volumes of blood from the ECMO pump and the LV, respectively. The position of the watershed zone was identified as the region along the descending aorta tract reaching the $VF = 50\%$ condition. The centroid of this region was calculated and its distance along the centerline from the RIA outlet surface ($d_{VF=50\%}$) was determined (Figure 1c).
Given their intrinsic correlation with the afterload [23], the systemic pressure mean ($\overline{P}_{sys}$) and range (ΔP_{sys}) were evaluated.
For the perfusion, the mean flow ($\overline{Q}_i$) was considered for each aortic vessel outlet.
For the evaluation of the ECMO trade-off level (Q^H_{ECMO}), the following steps were considered. Firstly, the trend of $\overline{Q}_i$ as a function of Q_{ECMO} was fitted with a linear model (Equation 2):

$$\overline{Q}_i(Q_{ECMO}) = k^i \cdot Q_{ECMO} + \overline{Q}^0_i \tag{2}$$

where k^i is the trend slope for the i-th outlet and $\overline{Q}^0_i$ is the mean flow in the i-th outlet in the no ECMO support condition. The goodness of this model was evaluated for each outlet and each case through the R^2 score. The $\overline{Q}_i$ for each of the 30 pathological scenarios was then compared with the corresponding value in the baseline healthy condition $\overline{Q}^H_i$. To establish the ECMO level to allow the perfusion at i-th outlet ($Q^H_{ECMO,i}$), the following condition, corresponding to the perfusion point, was imposed:

$$\overline{Q}_i(Q_{ECMO} = Q^H_{ECMO,i}) = \overline{Q}^H_i \tag{3}$$

Then, combing Equation 2 and Equation 3 it was possible to obtain $Q^H_{ECMO,i}$ for each outlet:

$$Q^H_{ECMO,i} = \frac{(\overline{Q}^H_i - \overline{Q}^0_i)}{k^i} \tag{4}$$

The $Q^H_{ECMO,i}$ is the ECMO level granting the perfusion at the i-th outlet. Then, to assess the ECMO trade-off level, it is sufficient to consider the artery requiring the highest level of ECMO among the different outlets, according to the condition of Equation 3. The ECMO trade-off level was calculated for each CS condition. Finally, a linear proportionality between Q^H_{ECMO} and p_{CS} was investigated, according to:

$$Q^H_{ECMO} = \Omega \cdot p_{CS} \tag{5}$$

where Ω is the proportionality factor. Similarly to the model of Equation 2, the fitting of the model of Equation 5 was evaluated in terms of R^2 score.

3 RESULTS

The VF maps at systolic peak are presented in Figure 2, for all CS and ECMO levels. The watershed zone position ($d_{VF=50\%}$) trends are presented in Figure 3.

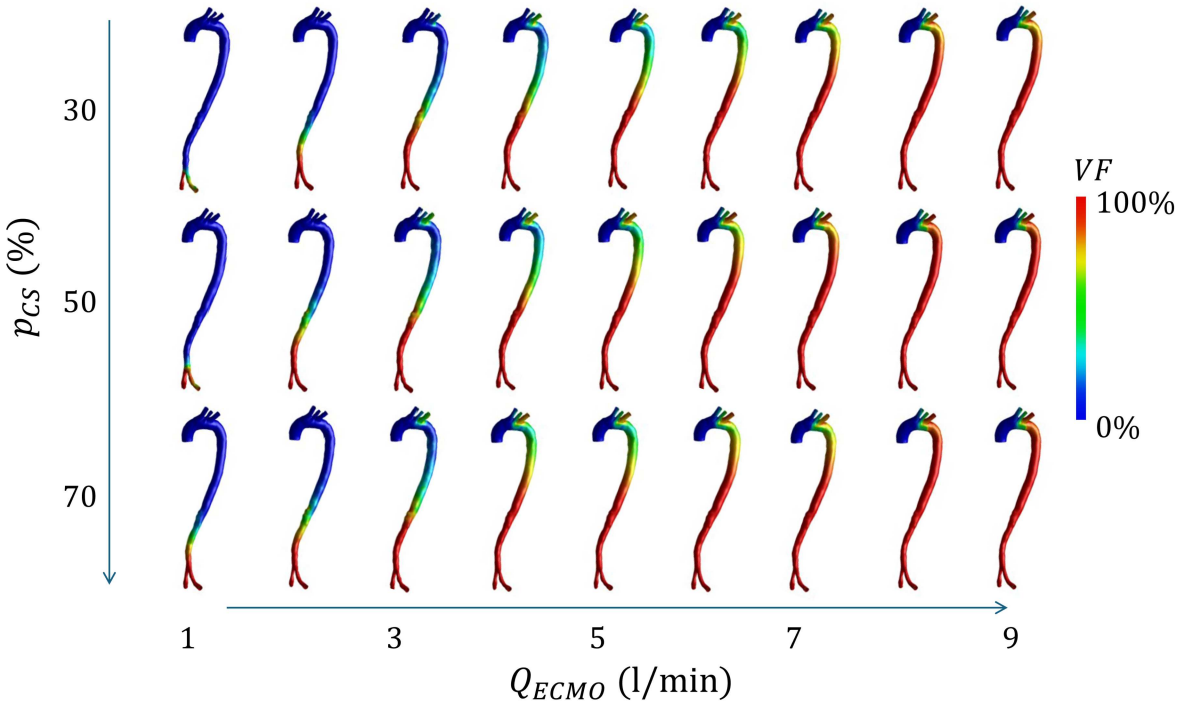

Figure 2: VF maps for the different simulated cases, according to the imposed levels of shock (p_{CS}) and ECMO levels (Q_{ECMO}).

The $\overline{P}_{sys}$ and the ΔP_{sys} parameters were evaluated as a function of ECMO level for each CS condition, as reported in Figure 4.

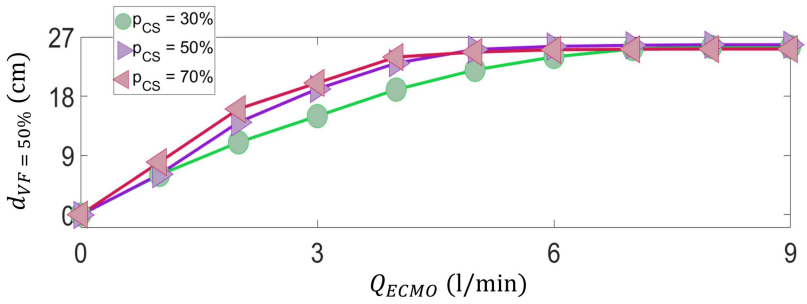

Figure 3: Watershed zone position ($d_{VF=50\%}$), as a function of ECMO level for the three CS conditions.

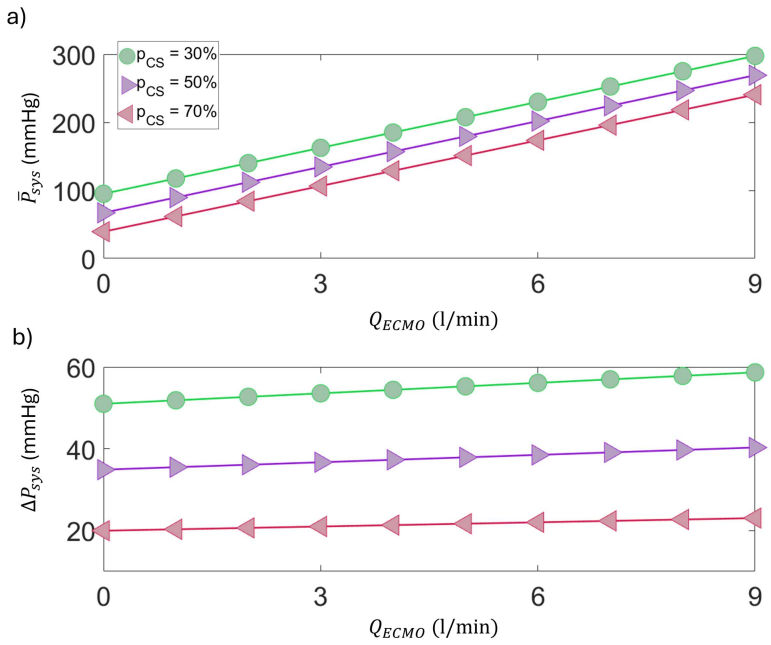

Figure 4: Behavior of $\overline{P}_{sys}$ (a) and ΔP_{sys} (b) as a function of ECMO level for the three CS conditions.

Finally, the $\overline{Q}_i$ as a function of ECMO level was reported in Figure 5 for each CS condition. The $\overline{Q}_i^H$ is reported in the graphs as well. The perfusion point ($\overline{Q}_i = \overline{Q}_i^H$) for each trend is highlighted with a cross in Figure 5. The linearity of each trend from Figure 5 was demonstrated with R^2 scores resulting to be >0.99 for each outlet.
The trade-off level Q_{ECMO}^H was evaluated by taking the highest ECMO level from the perfusion point among the outlets. From the results of Figure 5, it is possible to see that $\overline{Q}_{LIA}$ exhibited the highest perfusion points (Figure 5d) and thus they were used to estimate the Q_{ECMO}^H for the different shock values.
The ECMO trade-off levels are reported as a function of the CS percentage p_{CS} in Figure 6, together with the corresponding fitting according to the model of Equation 5. The fitting revealed a $R^2 = 0.991$ with an Ω factor equal to 4.9 l/min.

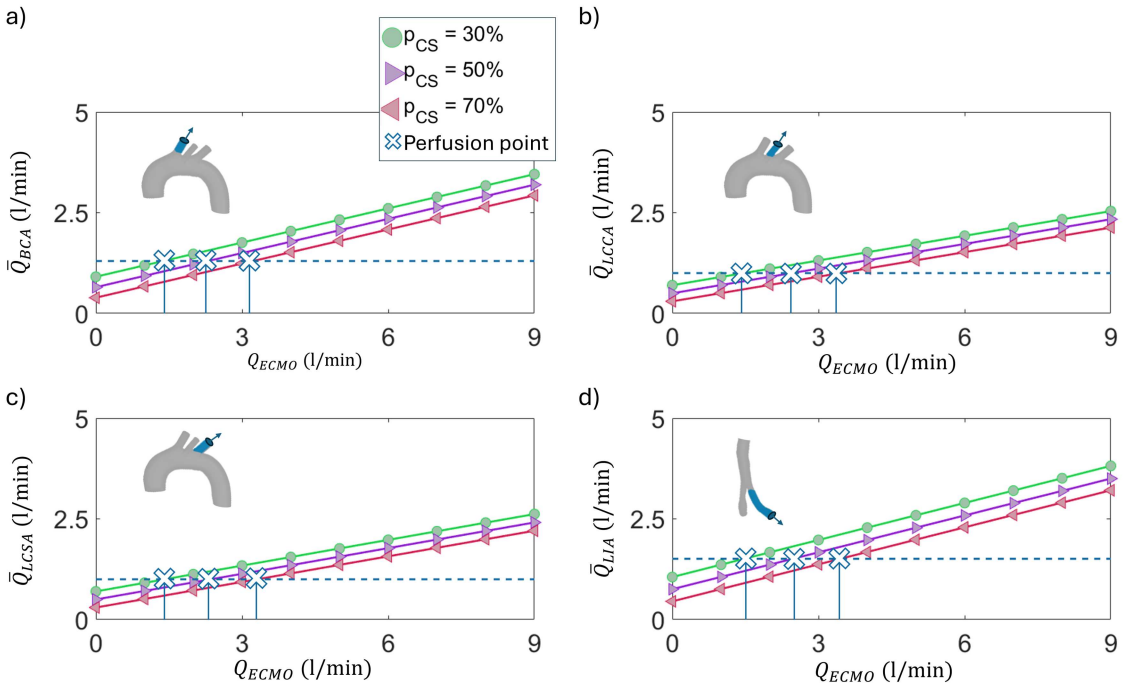

Figure 5: Behavior of $\overline{Q}_i$ as a function of ECMO level, for each CS condition at BCA (a), LCCA (b), LCSA (c) and LIA (d). Healthy flow levels from the baseline configuration are reported as dashed lines for each outlet.

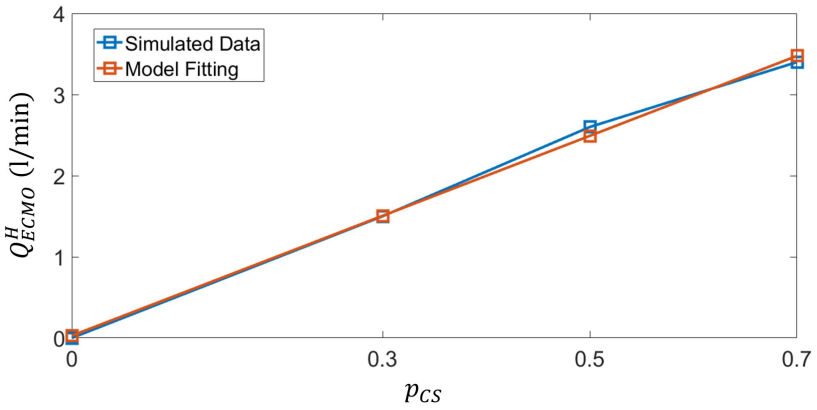

Figure 6: Trend of the ECMO trade-off level Q^H_{ECMO} as a function of shock percentage p_{CS}, with corresponding linear fitting.

4 DISCUSSION

The results presented in the previous section revealed the effects of ECMO support in different cardiogenic shock conditions. Particular focus was given on the position of the watershed zone, the afterload in terms of systemic pressure and the perfusion of the different arterial outlets of the aorta. By considering the healthy status simulation as a baseline, it was possible to evaluate

the perfusion point for each outlet in each pathological condition. From these data processing, we were able to define a trade-off level to allow the minimum level of ECMO to grant the overall perfusion and thus avoid higher levels, linked with unwanted afterload increases.
The volume fraction distribution maps of Figure 2 revealed the VF parameter behavior at systolic peak for all the different configurations. It is possible to observe that the mixing occurs at arch level only for $Q_{ECMO} > 7$ l/min. This phenomenon is in line with the retrograde nature of ECMO flow, already observed in other numerical studies [13]. The mixing reaches the arch for lower levels of ECMO support in the 70% shock condition. The same trend is quantified by the mixing point position, as represented in the graphs of Figure 3. This behavior can be linked to the fact that, when the shock is mild, the native flow from LV pushes the mixing zone back towards the descending aorta [19].
The pressure behavior is reported in Figure 4. As it was expected, the mean systemic pressure rises significantly with the ECMO level (Figure 4a). The worst condition was reached with the maximum systemic pressure of 300 mmHg for the level of CS equal to 30%. The same trend was already reported in the state of the art and in the clinical practice [24, 18], given the fact that the mean systemic pressure is linked with the LV afterload [23, 25]. On the other hand, the systemic pressure range appears to be minimally influenced by the ECMO support (Figure 4b), regardless of the CS level. While the $\overline{P}_{sys}$ increases up to 200%, the ΔP_{sys} faced a maximum increase of 16% only.
Concerning the perfusion of the aortic arteries, the mean flow trends are reported in Figure 5. It is interesting to note that the $\overline{Q}_i$ behavior as a function of Q_{ECMO} always revealed a linear trend, with satisfactory fitting ($R^2 > 0.99$), regardless of the outlet and of the CS condition. Additionally, the perfusion point was reached for each outlet with the proposed range of ECMO support levels. From the perfusion points, it appears clear that LIA is the outlet requiring the highest levels of Q_{ECMO} to reestablish the healthy flow (Figure 5d). This holds true for all the three CS levels imposed and it underlines the fact that the LIA is actually the hardest vessel to bring up to the perfusion point. Basically, if the ECMO level is enough to perfuse the LIA, all the other outlets have reached or overtaken the perfusion point already. From this concept, the ECMO trade-off level Q^H_{ECMO} was defined as the Q_{ECMO} corresponding to the LIA perfusion point. The Q^H_{ECMO} trend as a function of p_{CS} was reported in Figure 6. It is significant to highlight the successful linear fitting, as it opens the possibility to have a tool to correlate the shock level with the trade-off ECMO level. As stated already, if the $Q_{ECMO} \geq Q^H_{ECMO}$ condition is maintained, the perfusion at each outlet is granted. However, if instead $Q_{ECMO} = Q^H_{ECMO}$ is imposed, it is possible to avoid unnecessary afterload increases. It was, in fact, demonstrated that the systemic pressure monotonically rises with the ECMO level, as already highlighted by the results of Figure 4. The individuation of the ECMO trade-off level addresses the clinical issue of afterload increase already highlighted in the clinical state of the art [8, 26].
In the state of the art, different groups have already adopted numerical tools to explore and better understand the VA-ECMO support system, nevertheless they were mainly focused on different issues like flow mixing phenomena and cannulation configurations [27, 16]. On the contrary, the current work tried to address the clinical issue of VA-ECMO support that is the balance between afterload increase and overall vessel perfusion. With the current work, the basis for a tool for the estimation of the best ECMO level support for the perfusion of the aortic vessels was explored.
There are different points of development and limitations that can be highlighted. The proposed

model does not account for the influence of afterload on the stroke volume produced by the LV. For this reason, the systemic pressure was considered as a surrogate parameter for the LV afterload, which is in accordance with the clinical reality. For the future, it would be interesting to include LV distensibility in the simulation model in order to account for the correlation between stroke volume and systemic pressure. An additional point of development would be to widen the test case population by considering different aortic morphologies and cannulation strategies. It would be, in fact, interesting to explore these new configurations and then evaluate if the observed linearities are maintained.

5 CONCLUSION

In the current manuscript, a numerical analysis of the VA-ECMO support system was presented. The proposed strategy aimed at observing the watershed zone behavior, the afterload and the aortic vessel trend in different cardiogenic shock and ECMO support level configurations. The work results were used to define a model to correlate the shock level with a ECMO trade-off level to grant the total perfusion of the arterial vessels and to avoid unwanted afterload increases. The reported evidences put the basis for the future development of a tool for the planning of the best ECMO strategy to support cardiogenic shock cases.

REFERENCES

[1] L. A. Mendes, M. H. Picard, L. A. Sleeper, C. R. Thompson, A. K. Jacobs, H. D. White, J. S. Hochman, R. Davidoff, Cardiogenic shock: predictors of outcome based on right and left ventricular size and function at presentation, Coronary artery disease 16 (4) (2005) 209–215.

[2] T. Sun, A. Guy, A. Sidhu, G. Finlayson, B. Grunau, L. Ding, S. Harle, L. Dewar, R. Cook, H. D. Kanji, Veno-arterial extracorporeal membrane oxygenation (va-ecmo) for emergency cardiac support, Journal of Critical Care 44 (2018) 31–38.

[3] H. Kim, S.-H. Lim, J. Hong, Y.-S. Hong, C. J. Lee, J.-H. Jung, S. Yu, Efficacy of veno-arterial extracorporeal membrane oxygenation in acute myocardial infarction with cardiogenic shock, Resuscitation 83 (8) (2012) 971–975.

[4] G. M. Raffa, M. Kowalewski, P. Meani, F. Follis, G. Martucci, A. Arcadipane, M. Pilato, J. Maessen, R. Lorusso, In-hospital outcomes after emergency or prophylactic veno-arterial extracorporeal membrane oxygenation during transcatheter aortic valve implantation: a comprehensive review of the literature, Perfusion 34 (5) (2019) 354–363.

[5] L. Falk, M. Sallisalmi, J. A. Lindholm, M. Lindfors, B. Frenckner, M. Broomé, L. M. Broman, Differential hypoxemia during venoarterial extracorporeal membrane oxygenation, Perfusion 34 (1_suppl) (2019) 22–29.

[6] C. Contento, A. Battisti, B. Agrò, M. De Marco, A. Iaiza, L. Pietraforte, P. Pisani, A. Proietti, E. Vitalini, A. Montalto, et al., A novel veno-arteriovenous extracorporeal membrane oxygenation with double pump for the treatment of harlequin syndrome, Perfusion 35 (1_suppl) (2020) 65–72.

[7] J. J. Russo, N. Aleksova, I. Pitcher, E. Couture, S. Parlow, M. Faraz, S. Visintini, T. Simard, P. Di Santo, R. Mathew, et al., Left ventricular unloading during extracorporeal membrane oxygenation in patients with cardiogenic shock, Journal of the American College of Cardiology 73 (6) (2019) 654–662.

[8] E. W. Grandin, J. I. Nunez, B. Willar, K. Kennedy, P. Rycus, J. E. Tonna, N. K. Kapur, S. Shaefi, A. R. Garan, Mechanical left ventricular unloading in patients undergoing venoarterial extracorporeal membrane oxygenation, Journal of the American College of Cardiology 79 (13) (2022) 1239–1250.

[9] S. Celi, E. Vignali, K. Capellini, E. Gasparotti, On the role and effects of uncertainties in cardiovascular in silico analyses, Frontiers in Medical Technology 3 (2021) 748908.

[10] A. Mariotti, E. Gasparotti, E. Vignali, P. Marchese, S. Celi, M. V. Salvetti, Integrating in-vivo data in cfd simulations and in in-vitro experiments of the hemodynamic in healthy and pathologic thoracic aorta, in: International Work-Conference on Bioinformatics and Biomedical Engineering, Springer, 2022, pp. 208–219.

[11] B. M. Fanni, M. N. Antonuccio, A. Pizzuto, S. Berti, G. Santoro, S. Celi, Uncertainty quantification in the in vivo image-based estimation of local elastic properties of vascular walls, Journal of Cardiovascular Development and Disease 10 (3) (2023) 109.

[12] F. R. Nezami, F. Khodaee, E. R. Edelman, S. P. Keller, A computational fluid dynamics study of the extracorporeal membrane oxygenation-failing heart circulation, ASAIO Journal 67 (3) (2021) 276–283.

[13] M. Khamooshi, A. Wickramarachchi, T. Byrne, M. Seman, D. F. Fletcher, A. Burrell, S. D. Gregory, Blood flow and emboli transport patterns during venoarterial extracorporeal membrane oxygenation: A computational fluid dynamics study, Computers in Biology and Medicine 172 (2024) 108263.

[14] A. Wickramarachchi, A. J. Burrell, A. F. Stephens, M. Šeman, A. Vatani, M. Khamooshi, J. Raman, R. Bellomo, S. D. Gregory, The effect of arterial cannula tip position on differential hypoxemia during venoarterial extracorporeal membrane oxygenation, Physical and Engineering Sciences in Medicine 46 (1) (2023) 119–129.

[15] F. Fiusco, J. Lemétayer, L. M. Broman, L. Prahl Wittberg, Effect of flow rate ratio and positioning on a lighthouse tip ecmo return cannula, Biomechanics and Modeling in Mechanobiology 22 (6) (2023) 1891–1899.

[16] F. Fiusco, F. Rorro, L. M. Broman, L. Prahl Wittberg, Numerical and experimental investigation of a lighthouse tip drainage cannula used in extracorporeal membrane oxygenation, Artificial Organs 47 (2) (2023) 330–341.

[17] A. Seetharaman, H. Keramati, K. Ramanathan, M. E Cove, S. Kim, K. J. Chua, H. L. Leo, Vortex dynamics of veno-arterial extracorporeal circulation: A computational fluid dynamics study, Physics of Fluids 33 (6) (2021).

[18] K. Gu, S. Gao, Z. Zhang, B. Ji, Y. Chang, Hemodynamic effect of pulsatile on blood flow distribution with va ecmo: A numerical study, Bioengineering 9 (10) (2022) 487.

[19] E. Vignali, E. Gasparotti, D. Haxhiademi, S. Celi, Fluid dynamic model for extracorporeal membrane oxygenation support and perfusion in cardiogenic shock, Physics of Fluids 35 (11) (2023).

[20] I. E. Vignon-Clementel, C. Figueroa, K. Jansen, C. Taylor, Outflow boundary conditions for 3d simulations of non-periodic blood flow and pressure fields in deformable arteries, Computer methods in biomechanics and biomedical engineering 13 (5) (2010) 625–640.

[21] E. Kardampiki, E. Vignali, D. Haxhiademi, D. Federici, E. Ferrante, S. Porziani, A. Chiappa, C. Groth, M. Cioffi, M. E. Biancolini, et al., The hemodynamic effect of modified blalock–taussig shunt morphologies: A computational analysis based on reduced order modeling, Electronics 11 (13) (2022) 1930.

[22] K. Capellini, E. Vignali, E. Costa, E. Gasparotti, M. E. Biancolini, L. Landini, V. Positano, S. Celi, Computational fluid dynamic study for ataa hemodynamics: an integrated image-based and radial basis functions mesh morphing approach, Journal of biomechanical engineering 140 (11) (2018) 111007.

[23] K. Sagar, L. Pelc, T. Rhyne, L. Wann, D. Waltier, Influence of heart rate, preload, afterload, and inotropic state on myocardial ultrasonic backscatter., Circulation 77 (2) (1988) 478–483.

[24] C. Grant Jr, J. B. Richards, M. Frakes, J. Cohen, S. R. Wilcox, Ecmo and right ventricular failure: review of the literature, Journal of Intensive Care Medicine 36 (3) (2021) 352–360.

[25] V. A. Bennett, H. D. Aya, M. Cecconi, Evaluation of cardiac function using heart-lung interactions, Annals of Translational Medicine 6 (18) (2018).

[26] S. M. Ezad, M. Ryan, D. W. Donker, F. Pappalardo, N. Barrett, L. Camporota, S. Price, N. K. Kapur, D. Perera, Unloading the left ventricle in venoarterial ecmo: in whom, when, and how?, Circulation 147 (16) (2023) 1237–1250.

[27] M. Stevens, F. Callaghan, P. Forrest, P. Bannon, S. Grieve, Flow mixing during peripheral veno-arterial extra corporeal membrane oxygenation–a simulation study, Journal of biomechanics 55 (2017) 64–70.